Proceedings of the E-MRS Fall Meeting, Symposium H: Warsaw, Poland, September 19–23, 2011

Technology of Ultrathin NbN and NbTiN Films for Superconducting Photodetectors

M. Guziewicz[a], W. Słysz[a], M. Borysiewicz[a], R. Kruszka[a], Z. Sidor[a], M. Juchniewicz[a], K. Golaszewska[a], J.Z. Domagala[a,b], W. Rzodkiewicz[a], J. Ratajczak[a], J. Bar[a], M. Wegrzecki[a] and R. Sobolewski[a,c]

[a]Institute of Electron Technology, al. Lotników 32/46, 02-668 Warsaw, Poland

[b]Institute of Physics, Polish Academy of Sciences, al. Lotników 32/46, 02-668 Warsaw, Poland

[c]Departments of Electrical and Computer Engineering and Physics and Astronomy, Materials Science Program and Laboratory for Laser Energetics, University of Rochester, Rochester, NY-14627-0231, USA

We report fabrication and characterization of ultrathin NbN and NbTiN films designed for superconducting photodetectors. Our NbN and NbTiN films were deposited on Al_2O_3 and Si single-crystal wafers by a high-temperature, reactive magnetron sputtering method and, subsequently, annealed at 1000 °C. The best, 18 nm thick NbN films deposited on sapphire exhibited the critical temperature of 15.0 K and the critical current density as high as $\approx 8 \times 10^6$ A/cm^2 at 4.8 K.

PACS: 74.62.Bf, 74.78.−w, 81.15.Cd, 81.15.Jj

1. Introduction

Superconducting single-photon detectors (SSPDs) based on NbN nanostripes [1, 2] have already been demonstrated to be the fastest and most sensitive optical and near-infrared photon counters [3, 4] and are expected to play a leading role in such applications as fiber-based quantum communications [5], optical information processing [6], free-space satellite communications [6], or medical diagnostics [7]. In a typical design, an SSPD is a $10\times$ 10 μm^2 meander consisting of an ultrathin (≈ 5 nm thick) and $100 \div 200$ nm wide NbN nanostripe. The detector operates far below the NbN critical temperature T_C (typically 4.2 K) and biased with a subcritical current [2]. Absorption of an optical photon generates a local destruction of superconductivity within the stripe (so-called hotspot formation) that grows until a resistive region is formed across the nanostripe, thus, producing a detectable voltage signal [2]. Apart from the highest possible T_C, the nanostripe critical current density J_C is the second most important parameter for the best SSPD performance, as it defines the operating bias current I_b. In addition, the SSPD detection efficiency has been demonstrated to be exponentially increasing function of I_b [4].

In our previous work [8], we presented our investigations on structural and superconducting transport properties of ultrathin NbN films deposited on various substrates suitable for both electronic and optoelectronic applications. This report is focused on the latest results of the state-of-the-art superconducting NbN films and the new fabrication thrust aimed at ultrathin NbTiN films, most recently successfully implemented in SSPDs [9].

2. Experimental procedures

Our NbN and NbTiN films were grown by high-temperature, reactive RF magnetron sputtering using a γ-1000C system from the Surrey Nanosystems Ltd. The NbN films were deposited from a 3-inch diameter Nb target at DC power of 220 W in N_2–Ar gas mixture at temperature of 850 °C. The NbTiN films were deposited from metallic Nb and Ti targets by co-sputtering. We used Al_2O_3 (0001) and Si(001) substrates. High purity of our films was achieved by using the 4N5 purity of metallic targets, 6N purity of process gases, as well as maintaining the background pressure of 10^{-8} mbar. The thicknesses of the studied layers varied from 6 nm to 20 nm and they were, subsequently, annealed at ≈ 1000 °C, using a rapid thermal annealing (RTA) process, in order to improve their superconducting properties.

Extensive structural characterization of our films was performed using X-ray diffraction and transmission electron microscopy (TEM) and atomic force microscopy (AFM). For high resolution XRD analysis, the PANalytical X'Pert MRD diffractometer, equipped with the X-ray mirror, Ge (400) hybrid monochromator, and PIXCEL detector in reflected beam line, was applied. The TEM specimens were prepared by a focused ion beam (FIB) tool from Helios Nanolab and observed using the JEOL 2100 microscope. The Veeco Innova SPM AFM in-

strument was applied to study surface roughness of our specimens.

3. Results and discussion

3.1. Transport properties of NbN films

Transport measurements showed that even a 6 nm thick NbN film was superconducting with T_C above 10 K. The highest $T_C = 15.0$ K was observed for 18 nm NbN films after they were subjected to an RTA process for 20 min.

A special nanostripe test structure was fabricated for investigation of the J_C dependence on temperature T, as is schematically shown in Fig. 1a. Stripes with widths varying from 600 nm to 15 μm, the fixed length of 30 μm, and Au contact pads were chosen. Figure 1b shows an SEM micrograph of a 600 nm wide stripe. The stripe pattern was transferred from a mask by photolithography using a ma-N 1407 photoresist and reactive ion etching in the CF/O_2 plasma at RF power of 70 W.

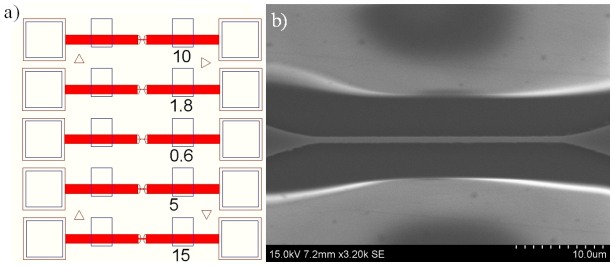

Fig. 1. (a) A photomask for a test structure used in $J_C(T)$ studies. The numbers indicate the given stripe width in μm. (b) A SEM micrograph of the narrowest (600 nm wide) stripe.

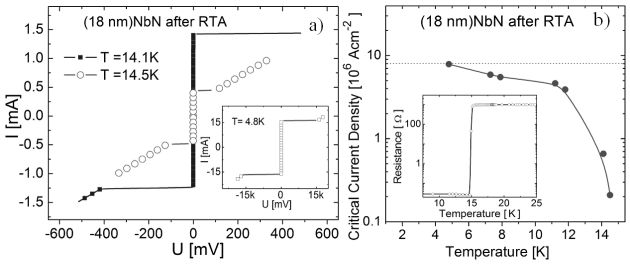

Fig. 2. (a) I–V characteristics of a tested NbN stripe. The inset shows the I–V curve taken at temperature $T = 4.8$ K. (b) The J_C vs. T dependence with the maximum 8 MA/cm^2 value marked. The inset shows R–T characteristics for the same sample.

Figure 2 presents a current–voltage (I–V) characteristics and $J_C(T)$ dependence measured for the above structure. In Fig. 2a we show the I–V curves thus below T_C and at the lowest studied temperature (inset), which was limited by DC current bias unit. We note that all our characteristics exhibit a very sharp superconducting-to--resistive transition with no measurable flux-flow region. In Fig. 2b, we demonstrate that for our best, 18 nm thick NbN film, J_C reaches 8 MA/cm^2 at $T = 4.8$ K, which is one of the highest values reported in literature, as, typically, I_b tends to be reduced by lithography process of the stripe patterning and some substrate flatness imperfections [10, 11]. We also note that even at $T = 14.5$ K, $J_C \approx 0.2$ MA/cm^2. The inset in Fig. 2a shows the resistive transition (R–T) of the same film, indicating that $T_C \approx 15$ K.

3.2. TEM studies of NbN films

A micrograph of a TEM cross-section of our 18 nm thick NbN film deposited on sapphire is presented in Fig. 3. A platinum layer visible on the top serves as a protection, used during the TEM specimen preparation. The cross-section shows an epitaxial growth of our film with the fcc structure, as well as atomically flat and very sharp interface. Some differences in the contrast levels of atomic-plane lines may suggest existence of oval grains at the upper part of the film. These were also observed in our previous AFM surface studies [8], as convex bows and can explain as the surface roughness after the RTA annealing. However, annealing at 1000 °C clearly improves the film crystallization process, and, in consequence, leads to the reported high values of both J_C and T_C.

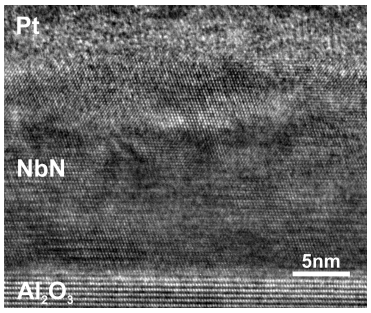

Fig. 3. A TEM cross-section of our NbN film indicating high level of epitaxy in the film.

3.3. Superconducting and structural properties of NbTiN films

We have studied transport properties of a nominally 20 nm thick NbTiN film deposited from separate Nb and Ti metallic targets (power 220 W and 80 W, respectively) in the gas flow mixture N_2/Ar of the total pressure of 8 μbar. Figure 4 shows the R–T characteristics before and after the RTA process, indicating the increase of T_C from 9.5 K up to 13 K after annealing at 1000 °C in Ar, the effect similar to that earlier observed in NbN films [8].

We have also performed extensive structural characterization studies of our NbTiN films and compared them directly to those earlier done for the NbN films [8]. X-ray

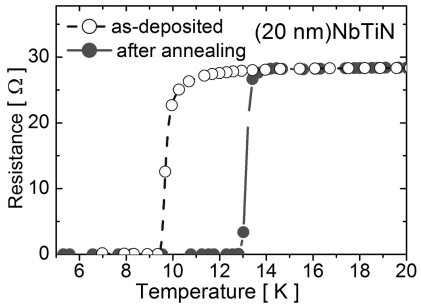

Fig. 4. The R–T dependence for a 20 nm thick NbTiN film deposited on a sapphire substrate before and after the RTA process performed in Ar at 1000 °C for 20 min.

characterization was performed using the Pixcel detector working in a stripe mode. The resulting $2\theta/\omega$ scan for the 111 reflection is shown in Fig. 5a. The scan has a highly symmetrical shape and reveals the characteristic "thickness" oscillations that indicate the actual film thickness of 15.3 nm and a good-quality film–substrate interface. The NbTiN lattice parameter $a = 4.37$ Å was calculated from the 111 peak position, assuming a relaxed cubic lattice unit. The value is very close to the 4.368 Å value previously obtained for as-deposited NbN [8], but it is lower than 4.389 Å reported for NbTiN by others [11]. We believe that the latter might be due to a nonuniform substitution of smaller Ti atoms into Nb positions. The rocking curve (not shown here) of the 111 reflection measured with the analyzer resulted in the full width at half maximum (FWHM) of 10 arcsec (≈ 0.05 mrad), which was at the resolution limit of our apparatus and indicated an excellent crystalline quality of our specimen.

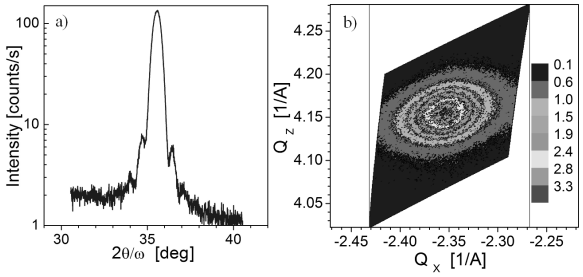

Fig. 5. The $2\theta/\omega$ spectrum of the 111 reflection of a studied NbTiN film. (b) The RSM image of the 311 NbTiN Bragg reflection. The diagram represents intensity scale in the range of $0.1 \div 3.3$ counts/s. The maxima of intensities are located at center of the pattern.

The applied detector mode allowed to collect independently our NbTiN film, an asymmetric reciprocal space map (RSM) of the 311 Bragg reflection and establish, if the lattice unit cell of the crystal was deformed or not. The RSM image shown in Fig. 5b proves perfect ordering of the (311) plane and confirms that the NbTiN film grown by us is of high quality. Finally, the AFM studies (see Fig. 6) performed on the thinnest, 6 nm film

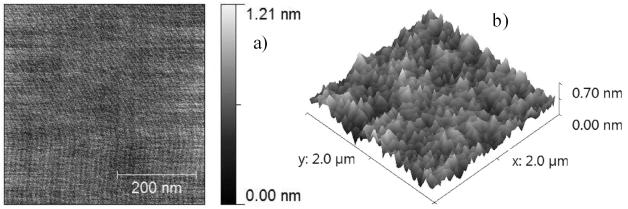

Fig. 6. AFM images of (6 nm)NbTiN film deposited on sapphire and RTA processed at 1000 °C in Ar for 20 min.

indicated on a very smooth surface with the roughness of 0.1 nm even after the RTA processing. There are no sharp, spike-like structures as were observed in NbN films [8].

4. Conclusions

We have demonstrated that 18 nm thick NbN films grown on a sapphire substrate at optimized sputtering and annealing conditions are essentially epitaxial and exhibit excellent superconducting transport properties with T_C as high as 15.0 K and J_C reaching 8 MA/cm^2 at 4.8 K. Our early fabrication and characterization studies of ultrathin NbTiN films grown by the co-sputtering process from Nb and Ti targets in reactive plasma confirm that indeed NbTiN has a very high potential for SSPD applications. The NbTiN films grow in an epitaxial manner and exhibit exceptionally high surface smoothness, even after RTA processing. After annealing optimization their superconducting transport properties should be as good as those of NbN.

Acknowledgments

The authors thank I. Zaytseva for her contribution in measurements. The work was supported in part by the European Regional Development Fund (Innovative Economy, POIG.01.01.02-00-108/09). R.S. thanks the Spanish Ministry of Education and the University of Salamanca for their financial support and hospitality during his one-semester-long research visit in Salamanca, Spain.

References

[1] G.N. Gol'tsman, O. Okunev, G. Chulkova, A. Lipatov, A. Semenov, K. Smirnov, B. Voronov, A. Dzardanov, C. Williams, R. Sobolewski, *Appl. Phys. Lett.* **79**, 705 (2001).

[2] R. Sobolewski, A. Verevkin, G.N. Gol'tsman, A. Lipatov, K. Wilsher, *IEEE Trans. Appl. Supercond.* **13**, 1151 (2003).

[3] A. Verevkin, J. Zhang, R. Sobolewski, A. Lipatov, O. Okunev, G. Chulkova, A. Korneev, K. Smirnov, G.N. Gol'tsman, A. Semenov, *Appl. Phys. Lett.* **80**, 4687 (2002).

[4] A. Korneev, P. Kouminov, V. Izbenko, G. Chulkova, K. Smirnov, B. Voronov, G.N. Gol'tsman, M. Currie, W. Lo, K. Wilsher, J. Zhang, W. Slysz, A. Pearlman, A. Verevkin, R. Sobolewski, *Appl. Phys. Lett.* **84**, 5338 (2004).

[5] W. Słysz, M. Węgrzecki, J. Bar, P. Grabiec, M. Górska, V. Zwiller, C. Latta, P. Bohi, I. Milostnaya, A. Korneev, O. Minayeva, G. Chulkova, K. Smirnov, B. Voronov, G. Gol'tsman, A. Pearlman, A. Cross, I. Komissarov, A. Verevkin, R. Sobolewski, *Appl. Phys. Lett.* **88**, 261113 (2006).

[6] J. Chen, J.B. Altepeter, M. Medic, K.F. Lee, B. Gokden, R.H. Hadfield, S.W. Nam, P. Kumar, *Phys. Rev. Lett.* **100**, 133603 (2008).

[7] M.T. Jarvi, M.J. Niedre, M.S. Patterson, B.C. Wilson, *Photochem. Photobiol.* **82**, 1198 (2006).

[8] W. Słysz, M. Guziewicz, M. Borysiewicz, J.Z. Domagała, I. Pasternak, K. Hejduk, W. Rzodkiewicz, J. Ratajczak, J. Bar, M. Wegrzecki, P. Grabiec, R. Grodecki, I. Wegrzecka, R. Sobolewski, *Acta Phys. Pol. A* **120**, 200 (2011).

[9] M.G. Tanner, C.M. Natarajan, V.K. Pottapenjara, J.A. O'Connor, R.J. Warburton, R.H. Hadfield, B. Baek, S. Nam, S.N. Dorenbos, E. Bermúdez Ureña, T. Zijlstra, T.M. Klapwijk, V. Zwiller, *Appl. Phys. Lett.* **96**, 221109 (2010).

[10] N. Marrocco, G.P. Pepe, A. Capretti, L. Parlato, V. Pagliarulo, G. Peluso, A. Barone, R. Cristiano, M. Ejrnaes, A. Casaburi, N. Kashiwazaki, T. Taino, H. Myoren, R. Sobolewski, *Appl. Phys. Lett.* **97**, 092504 (2010).

[11] J.R. Gao, M. Hajenius, F.D. Tichelaar, T.M. Klapwijk, B. Voronov, E. Grishin, G.N. Gol'tsman, C.A. Zorman, M. Mehregany, *Appl. Phys. Lett.* **91**, 062504 (2007).